Journal of Materials Chemistry A

RSC Publishing

PAPER

View Article Online
View Journal | View Issue

Cite this: J. Mater. Chem. A, 2013, 1, 8190

A comprehensive study of the crystallization of Cu–As–Te glasses: microstructure and thermoelectric properties

J. B. Vaney,[ab] G. Delaizir,[c] E. Alleno,[d] O. Rouleau,[d] A. Piarristeguy,[b] J. Monnier,[d] C. Godart,[d] M. Ribes,[b] R. Escalier,[b] A. Pradel,*[b] A. P. Gonçalves,[e] E. B. Lopes,[e] G. J. Cuello,[f] P. Ziolkowski,[g] E. Müller,[g] C. Candolfi,[a] A. Dauscher[a] and B. Lenoir[a]

Received 21st March 2013
Accepted 10th May 2013

DOI: 10.1039/c3ta11159h

www.rsc.org/MaterialsA

We report a thorough experimental study on the microstructure, thermal behavior and thermoelectric properties of the amorphous composition $Cu_{15}As_{30}Te_{55}$ and the glass–ceramics related-compounds synthesized by using the Spark Plasma Sintering (SPS) technique. Varying the conditions of the SPS process enables the synthesis of composite glassy-crystalline samples with different crystal/glass ratios. Such treatments result in complex microstructures composed of large glassy domains where nanocrystals of the metastable β-As_2Te_3 phase are embedded. These domains are separated by regions of the dendritic crystalline phase surrounded by a Cu-rich glassy matrix. The presence of β-As_2Te_3, confirmed by both powder X-ray diffraction and scanning electron microscopy, suggests that pressure and/or internal stresses play an important role in stabilizing this phase. This conclusion is further supported by neutron thermodiffraction experiments revealing a sharp crossover from the β-As_2Te_3 to the stable α-As_2Te_3 phase at temperatures below that of the SPS treatment. Transport properties measurements show that the presence of a crystalline fraction significantly lowers the electrical resistivity by four orders of magnitude. However, the probable intrinsic n-type behavior of β-As_2Te_3 has a detrimental influence on the thermopower values. Even though the partial crystallization of the glassy matrix leads to an increase in the thermal conductivity, the measured values remain on the order of 1 W m^{-1} K^{-1} at 300 K. Besides an overall increase in the dimensionless figure of merit *ZT*, our results demonstrate that the partial crystallization of an amorphous matrix is an efficient tool to tune the electrical resistivity over several orders of magnitude while maintaining low thermal conductivity values.

1 Introduction

Thermoelectric materials offer an effective way to convert thermal energy into electrical energy (Seebeck effect) and, reciprocally, electrical energy into thermal energy (Peltier effect). The performance of thermoelectric devices is directly related to the materials' dimensionless thermoelectric figure of merit *ZT* defined by $ZT = \frac{\alpha^2 T}{\rho\lambda} = \frac{PT}{\lambda}$ where T is the absolute temperature, α is the Seebeck coefficient (or thermopower), $P = \alpha^2/\rho$ is the power factor, ρ is the electrical resistivity and λ is the total thermal conductivity.[1]

A good thermoelectric material should display simultaneously a large thermopower, a low electrical resistivity and a low thermal conductivity. However, these three transport properties are mutually interdependent *via* the carrier concentration, making the optimization of the thermoelectric properties a complex task. In most thermoelectric materials, optimum power factors are obtained when the carrier concentration ranges between 10^{18} and 10^{21} cm^{-3} at room temperature *i.e.* in heavily doped crystalline semiconductors or semimetals.[2,3] Another key ingredient leading to highly thermoelectric materials is their complex crystalline structure that enables the thermal conductivity values to be lowered. Several strategies are usually employed to disrupt more efficiently the heat-carrying acoustic phonons either on an atomic or a microscopic scale. The former possibilities include mass fluctuations upon alloying or the presence of loosely bound atoms in oversized atomic cages.[3] Nanostructuring is at the heart of the latter approach through a combination of a micron-sized matrix embedding nanoscale precipitates across multiple length scales.[4–7]

[a]Institut Jean Lamour (IJL), UMR 7198 CNRS-Université de Lorraine, France
[b]Institut Charles Gerhardt (ICG), UMR 5253 CNRS-Université Montpellier 2, France. E-mail: annie.pradel@univ-montp2.fr
[c]Sciences des Procédés Céramique et de Traitement de Surface (SPCTS), UMR CNRS 7315, Centre Européen de la Céramique, Limoges, France
[d]Institut de Chimie et des Matériaux de Paris Est (ICMPE), UMR 7182 CNRS, CMTR, Thiais, France
[e]ST/ITN Instituto Superior Técnico, Universidade Técnica de Lisboa, P-2686-953 Sacavém, Portugal
[f]Institut Laue Langevin, 6 rue Jules Horowitz, B. P. 156, 38042 Grenoble, France
[g]Institute of Materials Research, German Aerospace Center (DLR) Linder Hoehe, D-51147, Cologne, Germany

A radically different strategy may be adopted by focusing on materials exhibiting intrinsically very low thermal conductivity values leaving P the only relevant parameter to be optimized. Organic amorphous materials like conducting polymers have been attracting a great deal of attention in recent years for their promising thermoelectric properties around room temperature.[8–10] Inorganic glassy materials also offer this possibility since their ability to conduct heat is hampered by their inherent disorder. In addition, the plethora of chemical compositions achievable allows their electronic properties to be tuned from metallic-like to semiconducting-like, for instance, in glasses based on chalcogenides (S, Se, Te) and/or pnictides (As, Sb, Bi, *etc.*).[11] However, one of the main obstacles to considering them for thermoelectric applications is their high electrical resistivity, which has so far prevented large ZT values from being achieved.

A fine control of the electrical resistivity therefore appears as the most challenging problem to be overcome before further considering these materials as potential thermoelectric materials. Though a first possibility would consist in varying the compositions to control the carrier concentration as in their crystalline analogues, a precise knowledge of the exact coordination number of the atoms is difficult to achieve. Another strategy relies on a controlled partial crystallization of the glassy matrix to lower the electrical resistivity. Provided a precise control of the fraction of the crystalline phase can be obtained, this innovative approach might help to improve the thermoelectric properties and hence warrants further attention.

Here, we report detailed investigations on semiconducting chalcogenide glasses and glass–ceramics based on the Cu–As–Te system. More precisely, we focused on the glass composition $Cu_{15}As_{30}Te_{55}$ and studied the influence of the crystalline nature and fraction on its thermoelectric properties. The choice of this particular composition is based on two main characteristics suitable for the purpose of the present study. First, the synthesis of a pure amorphous form of this compound can be easily done using a conventional quenching method and thus does not need ultrafast-quenching techniques such as melt-spinning. Second, this glass composition has a very high electrical resistivity with respect to glasses containing higher Cu contents so that the influence of a crystallized fraction on ρ is expected to be exacerbated.

2 Experimental

The glassy samples were synthesized in silica tubes under secondary vacuum. Starting elements, As (Goodfellow, 99.99%), Te (5N+, 99.99%) and Cu (Sigma-Aldrich, 99.999%), were first weighed in stoichiometric quantities (to obtain a total batch of ~5 g) and introduced in a silica tube. The tube was subsequently evacuated, sealed and heated in a furnace with the low heating rate of 9 K h^{-1} up to 1123 K, held at this temperature for 2 h and eventually quenched in a salt–ice–water mixture. The resulting ingots were hand-ground to micron-sized powders.

The thermal behavior of the as-quenched samples was studied by Differential Scanning Calorimetry (DSC) performed using TA instrument Q100 equipment from room temperature up to 573 K using different heating rates ranging from 5 up to 40 K min^{-1}.

Spark Plasma Sintering (SPS) of the powders was realized with the Dr. Sinter 505 Syntex, the set-up belonging to the "Plate-forme de Frittage Ile de France" (Thiais, France). This technique allowed us to obtain both amorphous bulk samples as well as glass–ceramic composites. The amorphous powders were introduced in an 8 mm diameter graphite die. The SPS sintering temperature was checked by a thermocouple placed into the graphite die at about 6 mm from the sample. To gain further insights into the influence of this process on the crystalline fraction, we varied the dwell time parameter from 0 to 30 minutes at a temperature of 423 K or 433 K and under a pressure of either 50 MPa or 100 MPa.

The density of the different glass and glass–ceramics bulk samples was determined through the Archimedean principle using a Kern balance. This balance enables weighing solids in air (m_{air}) as well as in a solvent (in our case, water m_{water}). If the density of the buoyancy medium is known (ρ_0), the density of the solid (ρ) is calculated as follows:

$$\rho = \frac{m_{air}}{m_{air} - m_{water}}\rho_0 \quad (1)$$

The microstructure of both the amorphous and glass–ceramics bulk samples was investigated on fresh fracture along the cross-section using a LEO SEM-FEG microscope. The composition of crystalline and glassy phases was estimated using Energy Dispersive X-ray Spectroscopy (EDXS) on a polished cross-section surface.

To identify the crystalline phases, powder X-ray diffraction (PXRD) measurements on the surface of the SPS bulk samples were carried out at room temperature using a D8 Bruker diffractometer equipped with a Vantec 1D-detector. To derive the integral breadth of the X-ray line of the crystalline phase, a pattern was recorded in the 2θ range 10–90° with another D8 diffractometer equipped with a 1D-detector and a primary monochromator filtering the Cu-Kα_2 emission line. A good signal-to-noise ratio at large 2θ was obtained for a total recording time of 96 hours. The integral breadths of several lines were determined by fitting a Lorentzian profile on a background-subtracted pattern. The instrumental contribution to the integral breadth (β_i) was determined by a preliminary experiment on LaB_6 and subtracted from the observed integral breadth (β_0) to provide an estimated intrinsic sample broadening (β_e).

Neutron thermodiffraction was used to study the crystallization process occurring in the glasses upon heating. The neutron diffraction experiments were performed using the D1B instrument at the Institut Laue–Langevin in Grenoble (France) with a nominal wavelength of 2.52 Å. Two samples of compositions $Cu_{15}As_{30}Te_{55}$ and $Cu_{20}As_{20}Te_{60}$ were placed in non-sealed cylindrical vanadium containers in a vacuum (outer diameter of 8 mm and inner diameter of 7.6 mm). Using a standard ILL furnace (vertical top loading furnace), neutron diffraction spectra were continuously collected on samples subjected to the following heating ramps: from room temperature to 363 K at a rate of 5 K min^{-1} and then from 363 K to 473 K at a lower rate of 0.1 K min^{-1}. For the cooling process, the furnace was simply switched off to allow the samples to reach room temperature in 'free fall'.

Electrical resistivity measurements were performed on disk-shaped samples ($Ø \sim 8$ mm) using the van der Pauw technique.[12] The disks were then cut into bar-shaped samples ($\sim 1 \times 1 \times 8$ mm^3) for thermopower measurements performed under an argon atmosphere between 300 K and 360 K. The measurements were carried out at fixed temperatures using a home-made apparatus based on the differential method.[13] Stabilized positive and negative thermal gradients ($\Delta T \sim 2$ K) were applied by heating alternatively each end of the sample: the thermopower values were then obtained as an average of the forward and reverse values. The temperature gradient and thermoelectric voltage were measured by two n-type thermocouples pressed by mulite rods against one side of the sample.

Thermopower mapping was conducted under vacuum using a potential Seebeck microprobe (PSM) on a sample surface of 4×0.5 mm^2 with a resolution of 10×10 μm^2.[14] This measurement was performed on a glass–ceramic sample obtained at 423 K, 50 MPa, 30 min dwell time. The scan direction of the measurements was in the rising *x*-direction (typewriter style), beginning from zero for every new line. Contact detection was established by a load cell and a microcontroller giving a trigger signal to the transient recorder. The applied force at each measurement point was about 1.65 mN μm^{-2}. The elapsed time between the contact and the desired force-trigger was about 3 ms. For each point, two thermopower values were saved from different time domains. The measurement temperature is estimated to be 5 to 10 K above room temperature. Black fragments visible in the resulting maps along the measurement direction or as a single point are due to contact problems.

The thermal conductivity was determined at room temperature *via* thermal diffusivity measurements performed under an argon atmosphere on cylinder-shaped samples using LFA 427 (Netzsch) equipment. Both properties are related by the formula $\lambda = aC_p\rho_V$ where a is the thermal diffusivity, C_p is the specific heat and ρ_V is the density measured by the Archimedean principle as previously mentioned. Specific heat measurements (DSC 403 F3, Netzsch) were performed using the continuous scanning method under an argon atmosphere.

3 Results and discussion

3.1 Glass–ceramics formation and microstructure

The crystallization behavior of the $Cu_{15}As_{30}Te_{55}$ glass was investigated using DSC experiments. The thermograms presented in Fig. 1a show the evolution of thermodynamic properties up to 573 K using different heating rates ($\nu = 5$, 10, 20 and 40 K min^{-1}). Two characteristic temperatures are clearly observed on the DSC curves: the glass transition temperature T_g and the crystallization temperature T_p. Both temperatures increase with the heating rate. Increasing the heating rate from 5 K min^{-1} to 40 K min^{-1}, T_g and the first crystallization temperature T_{p1} shift from 394 K to 408 K and from 423 K to 441 K, respectively. According to Hruby,[15] the difference between these two temperatures ($T_{p1} - T_g$) can be used as a criterion to determine the thermal stability of a glass which is considered as stable when this difference exceeds 100 K. In the present case, a difference of ~30 K is obtained indicating that this glass is rather thermally unstable. The presence of two distinct exothermic peaks suggests that the crystallization of two different phases occurs. The peaks are better resolved at low heating rates *i.e.* at 5 or 10 K min^{-1}. The crystallization activation energy E_c can be inferred using the method introduced by Ozawa and specifically designed for non-isothermal study.[16] As shown in Fig. 1b, the value of E_c is deduced from the slope of ln ν plotted as a function of $1000/T_{p1}$ following the relation

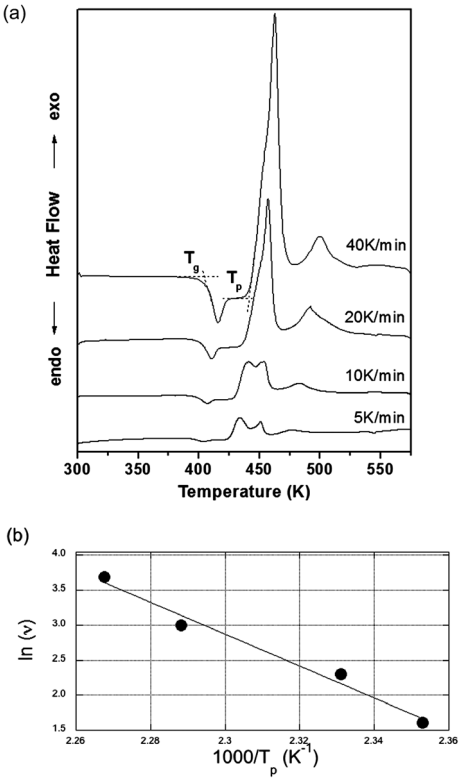

Fig. 1 (a) DSC curve of the $Cu_{15}As_{30}Te_{55}$ glass and (b) calculation of crystallization energy E_c using Ozawa's method.

$$\frac{d(\ln \nu)}{d\left(\frac{1}{T_{p1}}\right)} = -\frac{E_c}{R} \quad (2)$$

where R is the gas constant. The crystallization energy E_c of the first peak T_{p1} is equal to 189 kJ mol^{-1}. This low value suggests that the glass composition requires a small amount of energy to jump to the crystalline state, hence making the sample poorly stable and quite prone to crystallization.

The SPS parameters (pressure, temperature, vertical displacement of punches) during the sintering process are shown in Fig. 2. The sintering process starts around 373 K, becomes maximal at 413 K before ending at 423 K. It is generally assumed that the sintering of amorphous powders by SPS proceeds through a viscous flow mechanism.[17] For the synthesis of glass–ceramics, two mechanisms have been assumed. The first one associates the densification of glassy powder through viscous sintering to a subsequent devitrification of the matrix.[17] The second possible mechanism implies densification and concomitantly a gradual crystallization of the matrix through

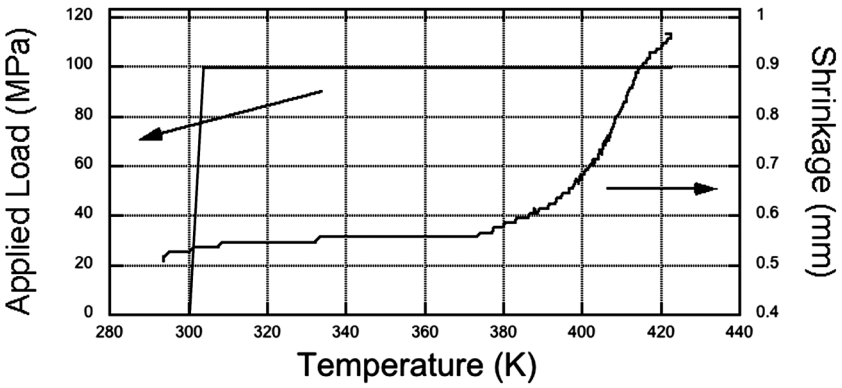

Fig. 2 Graph showing the pressure applied and shrinkage (in mm) as a function of temperature during SPS sintering of the $Cu_{15}As_{30}Te_{55}$ glassy powder.

the growth of a neck between glassy particles.[17] For a given glass composition, the amorphous phase has a considerably lower viscosity than the corresponding crystalline phase, so that the sintering of polycrystalline material is inevitably more difficult than its amorphous counterpart. This suggests that the first mechanism described above, *i.e.* achieving full density prior to any significant crystallization, is likely at play. Moreover, it is well known that the current distribution in the SPS die and through the sample is different in the case of a conductor and an insulating material.[18] In the case of a non-electrically conducting sample such as alumina or silica based glass, no Joule heating is expected through the sample so that the die ensures sample's heating. This contrasts with the case of conducting materials such as metals or metallic glasses, for which Joule heating starts immediately through the sample at the beginning of the process. Due to the semiconducting properties of the $Cu_{15}As_{30}Te_{55}$ glass composition,[19] we surmise that heating occurs through both the carbon die and the powder.

Based on the above considerations, a series of SPS experiments was carried out in order to obtain either a glass bulk material or glass–ceramics with different crystalline fractions. From the DSC data collected at the rate of 40 K min^{-1}, the sintering temperatures were chosen accordingly to lie between the glass transition and the first crystallization temperature *i.e.* 423 K or 433 K. Applied pressures of 50 and 100 MPa were selected and different dwell times were tested (0, 2, 5, 10 and 30 min) with the aim of varying the crystalline fraction.

The density of the glass bulk material was measured to be 5.9 g cm^{-3} when the conditions 100 MPa-423 K-no-dwell-time were applied (Table 1). This value compares well with that obtained on the initial glass synthesized by the conventional melt-quenching technique. The PXRD pattern of the obtained pellet was indeed that of an amorphous material (Fig. 3b) demonstrating that fully densified amorphous samples were successfully obtained by SPS treatment. Upon partial crystallization, the density increases to 6.30 ± 0.10 g cm^{-3} at the maximum

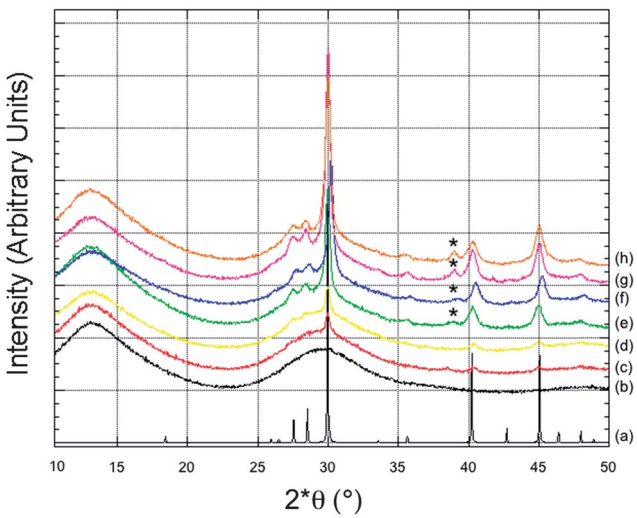

Fig. 3 XRD patterns of (a) β-As_2Te_3, glass and glass–ceramics sintered with the SPS parameters (b) 423 K, 100 MPa, 0 min, (c) 423 K, 100 MPa, 1 min, (d) 423 K, 100 MPa, 3 min, (e) 423 K, 100 MPa, 5 min, (f) 423 K, 100 MPa, 10 min, (g) 423 K, 100 MPa, 30 min, and (h) 433 K, 50 MPa, 2 min.

Table 1 Density, volume fraction of the biphasic domains, room temperature thermoelectric properties and crystalline fraction inferred from eqn (4) of the different SPS glasses and glass–ceramics

SPS parameters	0′-423 K-100 MPa	5′-423 K-100 MPa	10′-423 K-100 MPa	30′-423 K-100 MPa	2′-433 K-50 MPa
Density (g cm^{-3})	5.90 ± 0.1	6.03 ± 0.1	6.13 ± 0.1	6.23 ± 0.1	6.30 ± 0.1
Biphasic fraction (vol%)	0	53	67	80	89
ρ (mΩcm)	7.9 × 10^4	8.2	7.2	4.3	1.2
α (μV K^{-1})	870	70	72	69	55
Power factor (μW m^{-1} K^{-2})	1	60	72	111	257
λ (W m^{-1} K^{-1})	0.22	0.40	0.43	0.50	1.07
f_{crys} (vol%)	0	18	21	25	43
ZT (300 K)	0.001	0.004	0.050	0.060	0.072

crystalline fraction (433 K, 50 MPa, 2′ dwell time). As we shall see below, this result can be attributed to the crystallization of the β-As_2Te_3 compound that has a theoretical density of 6.29 g cm^{-3}.[20]

PXRD measurements were carried out to determine the nature of the phases crystallizing in the glassy matrix (Fig. 3c–h). The well-defined peaks showing up correspond to the crystallization of the β-As_2Te_3 phase (see Fig. 3a for its PXRD pattern). An additional small peak appearing at longer dwell time (marked by *) could not be unambiguously identified and might correspond to either α-As_2Te_3, AsTe or CuTe.

Fig. 4a–c show the EDXS measurements performed to obtain further information on the microstructure and its evolution with the SPS parameters. In the present case, a precise determination of the crystalline fraction is challenging given the different phases coexisting at the micron and sub-micron scales *i.e.* an amorphous phase containing well-crystallized nano-sized precipitates surrounded by biphasic regions composed of dendritic crystalline domains embedded in a glassy matrix. Thus, as a first estimation, only the relative part of each domain (amorphous and biphasic) was determined using image-analysis software on EDXS-SEM pictures. The percentage obtained should therefore be regarded as an upper bound of the actual crystalline fraction. Within this rough approximation, the results indicate an increase in the crystalline fraction as the dwell time increases up to 30 min under the same temperature and pressure conditions (Table 1). EDXS reveals that Te and As elements are homogeneously distributed in the material which is not the case for Cu (Fig. 5). Quantitative analyses of these crystals suggest that the chemical composition corresponds to As_2Te_3 without any detectable traces of Cu, further corroborating the indexation of the PXRD pattern. As a consequence, the remaining glassy domains are enriched in Cu compared to the composition of the initial amorphous phase. Based on these images, the crystallized nano-sized domains are estimated to be less than 100 nm.

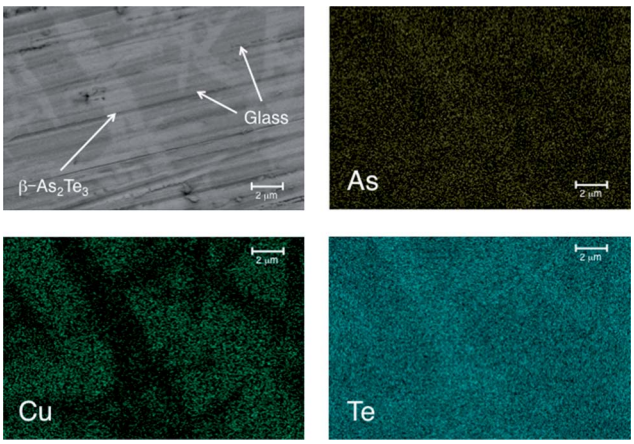

Fig. 5 Composition measured by EDXS revealing the presence of β-As_2Te_3 surrounded by a Cu-rich glassy matrix.

More intriguing is the fact that the β-form of As_2Te_3 crystallizes in the present case. While α-As_2Te_3 (monoclinic structure, space group $C2/m$)[20] is stable under ambient conditions and can be easily synthesized by conventional solid-state synthesis routes, the β-As_2Te_3 allotropic structure (rhombohedral structure of Bi_2Te_3 structure type, space group $R\bar{3}m$)[20–22] is metastable and so far could only be synthesized under high-pressure or by rapid quenching.[20–23] The fact that the metastable high-pressure β-As_2Te_3 phase is favored in the glass may be due to the constraint of the material through an applied pressure during the SPS process. It's well known that the β variety is denser than the stable α form.[23] Thus a phase transition β → α

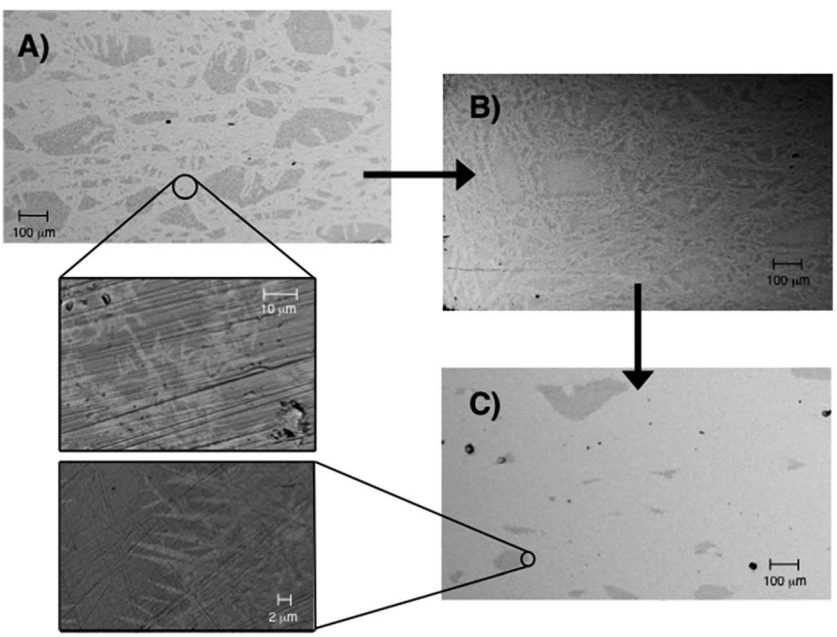

Fig. 4 SEM images of SPS glass and glass–ceramics showing the presence of dendritic crystallized structures in the glassy matrix for (a) 423 K, 100 MPa, 10 min, (b) 423 K, 100 MPa, 30 min, and (c) 433 K, 50 MPa, 2 min.

at room temperature would imply an increase in volume $\Delta V_{\beta\rightarrow\alpha} > 0$.[23] Since the β-$As_2Te_3$ crystals are embedded in the glassy matrix, this volume change is prevented in the present case.

This conclusion seems to be further corroborated by neutron thermodiffraction experiments carried out to determine not only the nature of the phase crystallizing in the glassy matrix but also their evolution upon heating. Fig. 6a and b show 3D plots of the entire set of data collected up to 473 K on the $Cu_{15}As_{30}Te_{55}$ and $Cu_{20}As_{20}Te_{60}$ glasses, respectively. Up to 405 K, both samples remain in an amorphous state without any discernable changes. Above this temperature, three distinct peaks are visible at 48.1°, 65.5° and 75.5° (Fig. 7a–c) and correspond to the three main reflections of the β-As_2Te_3 phase. Within a very narrow temperature window of ~2 K, the β-As_2Te_3 phase undergoes a structural transition to the α-type structure that does not show further evolution with temperature up to 473 K. These results clearly indicate a narrow domain of existence of the β-As_2Te_3 phase and show that, at temperatures at which the SPS treatment is performed (423 and 433 K), the α-As_2Te_3 phase should be predominant in the crystalline fraction of the composite sample. The applied pressure during the SPS process together with internal stresses thus likely plays an important role in the stabilization of the β phase.[23]

Upon closer inspection of Fig. 3 (patterns h and g), it can be noticed that, even in the most crystallized sample, the reflections corresponding to β-As_2Te_3 in the PXRD pattern are broad likely due to the size of the precipitates and/or microstrains. To determine which mechanism is at play here, the integral breadth of the reflections was evaluated based on PXRD data at higher resolution collected on the most-crystallized sample

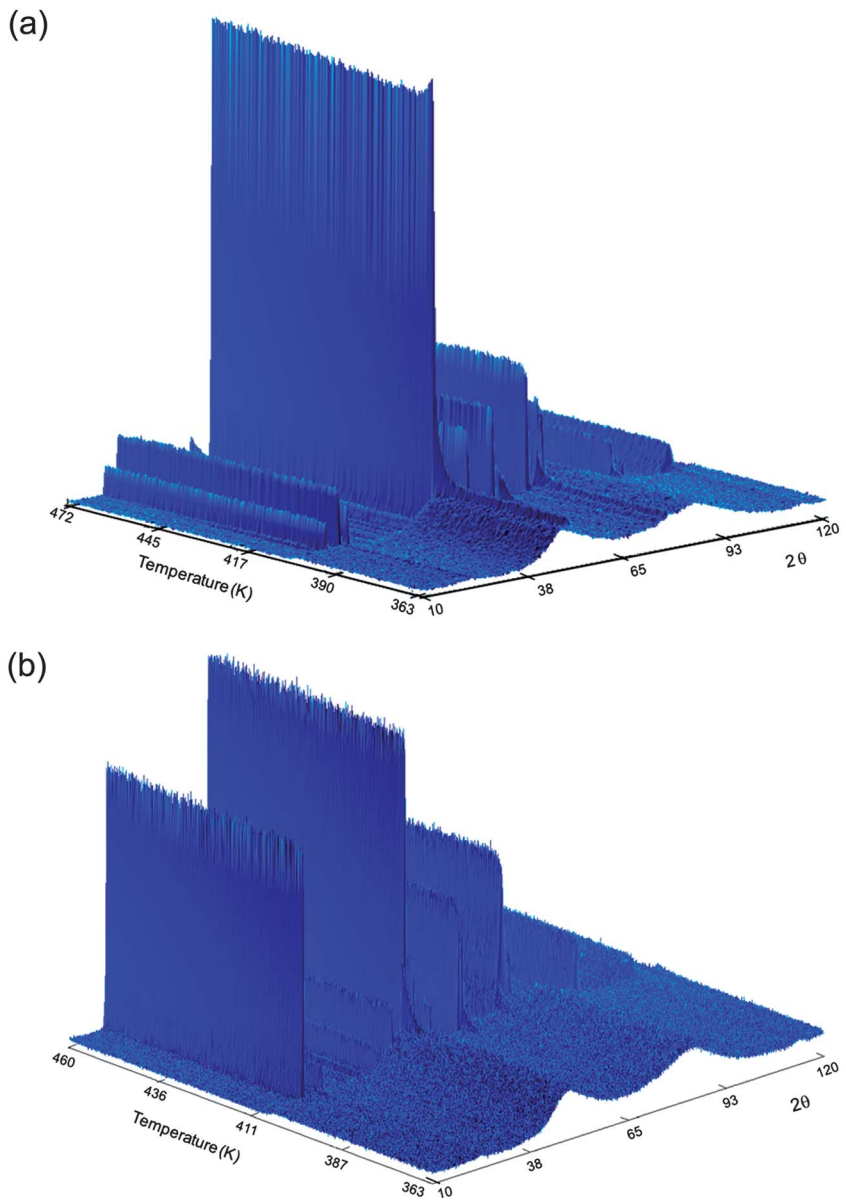

Fig. 6 3D plots of the powder thermodiffraction data collected between 10° and 120° as a function of temperature for the (a) $Cu_{15}As_{30}Te_{55}$ and (b) $Cu_{20}As_{20}Te_{60}$ samples.

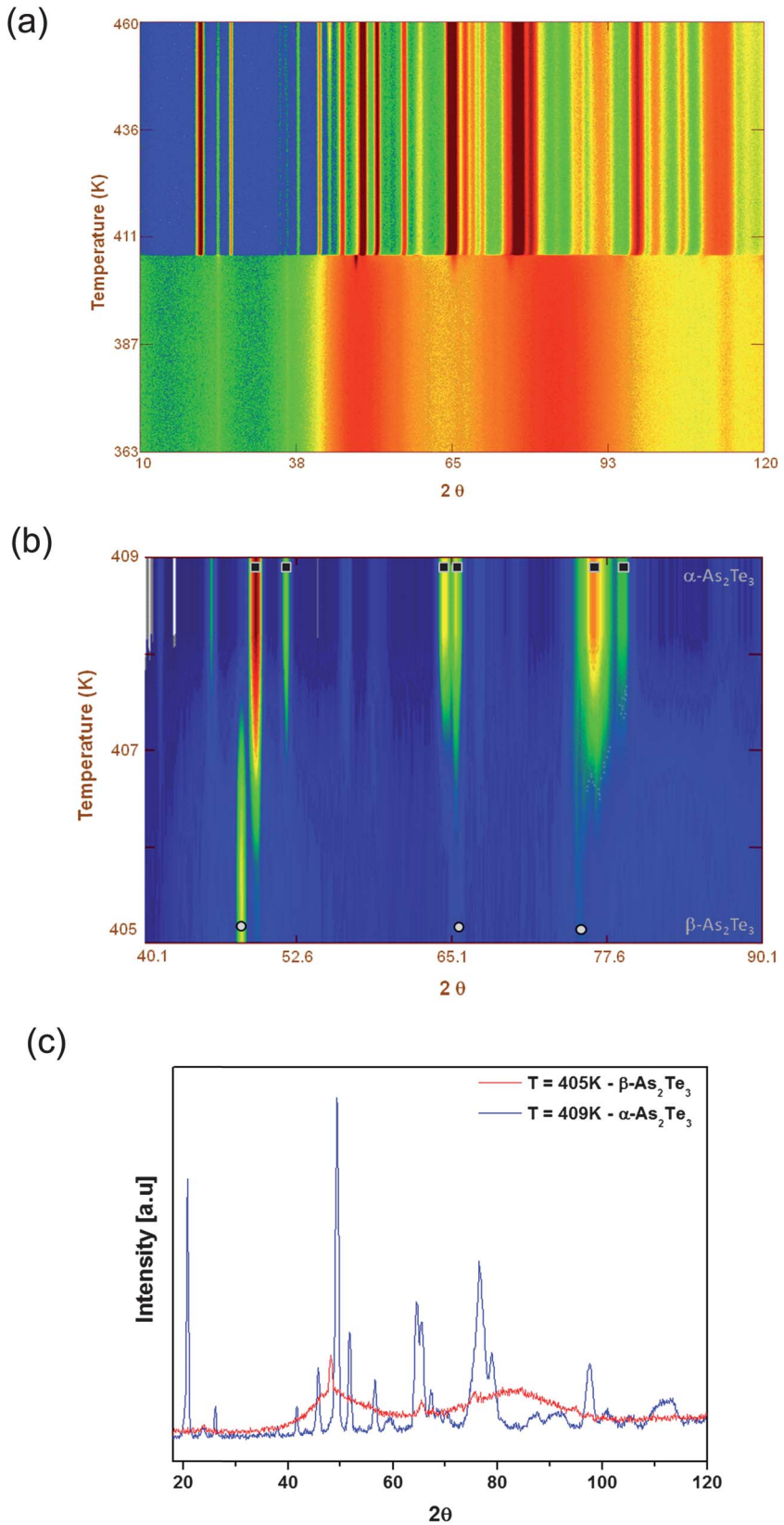

Fig. 7 (a) 2D mapping of the diffraction data of the $Cu_{20}As_{20}Te_{60}$ sample as a function of temperature showing the transition from the β-As_2Te_3 to the α-type structure that occurs near 409 K. (b) Magnification of the neutron thermodiffraction data near the β–α phase transition. The main reflections of the β and α phases are marked by a white circle and a black square, respectively. (c) Neutron powder diffraction pattern highlighting the structural transition that sets in between 405 and 409 K.

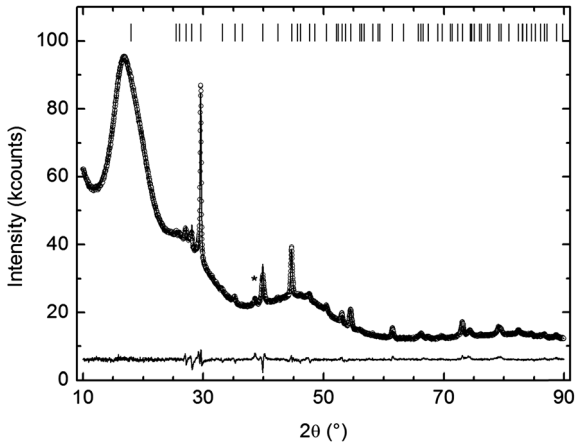

Fig. 8 Rietveld refinement of the high-resolution X-ray powder pattern (see text for explanations) of the sample labeled (h) in Fig. 3. The open circles are the experimental data, the line is the calculated pattern, the bottom line is the difference pattern (exp. − calc.) and the upper ticks are the Bragg angles corresponding to β-As_2Te_3. The main reflection of the second phase is labeled by a star.

(Fig. 8). The so-called Williamson–Hall relation then allows separating the size (D_v, volume-weighted column length) from the microstrain (ε, maximum strain) broadening.[24] These two quantities are related to the intrinsic integral breadth by:

$$\frac{\beta_e \cos\theta}{\lambda} = \frac{4\varepsilon \sin\theta}{\lambda} + \frac{1}{D_v} \quad (3)$$

where λ is the wavelength of the CuKα radiation. As shown in Fig. 9, $\frac{\beta_e \cos\theta}{\lambda}$ clearly varies linearly with the scattering vector $\frac{2\sin\theta}{\lambda}$. A linear fit against the experimental data with D_v and ε as fitting parameters yields $D_v = 80 \pm 30$ nm and $\varepsilon = 0.29\% \pm 0.06\%$. A better estimation of both D_v and ε was derived from Rietveld refinements of the pattern using the Fullprof software.[25] This method enables a more reliable analysis of the microstructural effects by fitting each reflection to a pseudo-Voigt function, unlike the Williamson–Hall plot where a Lorentzian profile is assumed. In the literature, two Bi_2Te_3-type structures were reported for β-As_2Te_3 by Shu *et al.*[21,22] These two models differ by slightly different positions of the As and Te atoms. We initially refined the experimental data considering both structures. In each case, the positions of the atoms and the lattice parameters were kept constant and the size and strain parameters were solely allowed to vary. Since a better agreement was found with the structure reported by Shu *et al.*[22] in 1986 (*R*-factors of $R_B = 21.5\%$ and $R_B = 31.3\%$, respectively), refinements were pursued with this structure. In a second step, the positions of the atoms were released. The best refinement (Fig. 8) led to $D_v = 73$ nm and $\varepsilon = 0.28\%$ (*R*-factors of $R_p = 0.9\%$ and $R_B = 13.7\%$). As a consistency check, the same analysis was repeated in another part of the sample and yielded very similar values ($D_v = 82$ nm and $\varepsilon = 0.39\%$). While the size of the crystalline domain of metastable β-As_2Te_3 – found to be small – is consistent with EDXS analyses, the value of the strain parameter is more surprising. Such a high value, similar to that found in ball-milled molybdenum (0.4%) for instance,[26] may be considered as evidence of the presence of strong internal stresses stabilizing the β form of the As_2Te_3 compound.

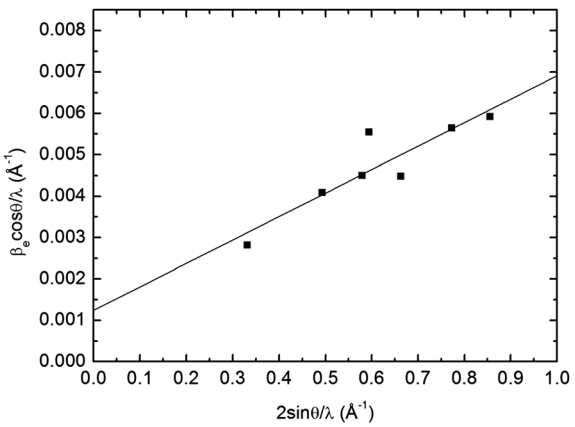

Fig. 9 Williamson–Hall plot of the sample integral breadth (β_e) as a function of the scattering vector length. The solid squares stand for the experimental data while the solid black line is the best fit to the data according to eqn (2).

3.2 Thermoelectric properties

Fig. 10 shows the temperature dependence of the electrical resistivity of the glass and glass–ceramic samples. The ρ values of the amorphous parent compound reach about 1 Ωm at 300 K, in line with previous results.[19] The electrical resistivity decreases by 4 orders of magnitude when crystals of β-As_2Te_3 are present in the glassy matrix. This decrease mainly originates from the presence of the crystalline phase rather than an enhancement of the copper enriched amorphous phase since the decrease is almost twice that observed in pure As–Te–Cu glasses with different Cu content.[27] As mentioned above, As_2Te_3 crystallizes in two allotropic forms consisting of either a rhombohedral structure (β-As_2Te_3) or a monoclinic structure (α-As_2Te_3). α-As_2Te_3 exhibits at 300 K high thermoelectric power

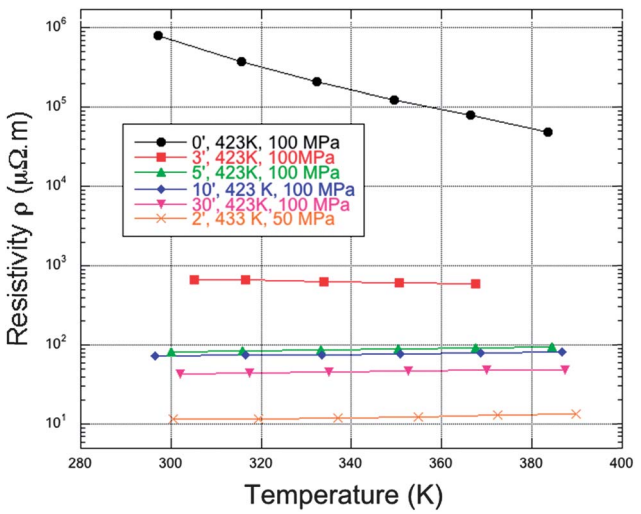

Fig. 10 Electrical resistivity as a function of temperature for different SPS glass and glass–ceramics samples.

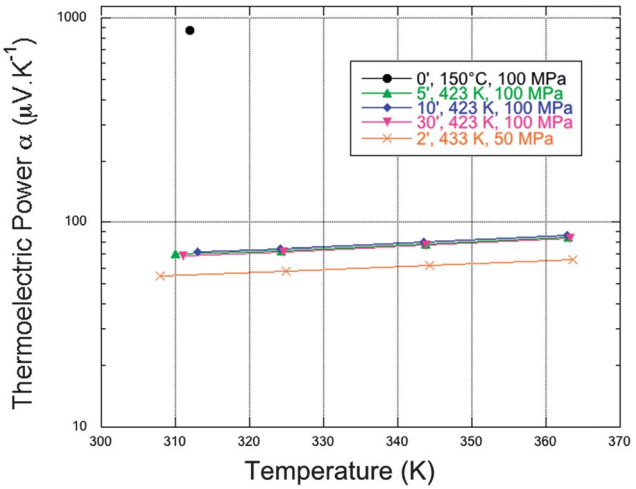

Fig. 11 Thermopower as a function of temperature for different glass and glass–ceramic samples.

(ranging between −230 and −260 μV K^{-1}), low thermal conductivity (estimated to 4.0 W m^{-1} K^{-1}) and an electrical resistivity value of 40 μΩ m.[20,28] Though the thermopower values of β-As_2Te_3 remain so far unknown, it might show similar α values due to the strong similarities in the crystal and electronic structures of both compounds.[29]

Regardless of the crystalline fraction, α slowly increases with temperature up to 365 K and shows positive values indicating that all the samples are p-type materials (Fig. 11). The $Cu_{15}As_{30}Te_{55}$ parent glass exhibits the highest α value reaching 900 μV K^{-1} at 315 K. The presence of crystalline β-As_2Te_3 in the glassy matrix markedly influences the values of α that drop to 70 μV K^{-1} at the maximum crystalline fraction. While the strong decrease in the ρ values may be the main factor lowering α as is usually observed in crystalline semiconductors, the type of charge carriers dominating the electronic transport in β-As_2Te_3 may also play a significant role. When both electrons and holes contribute to the electrical conduction, α decreases due to the

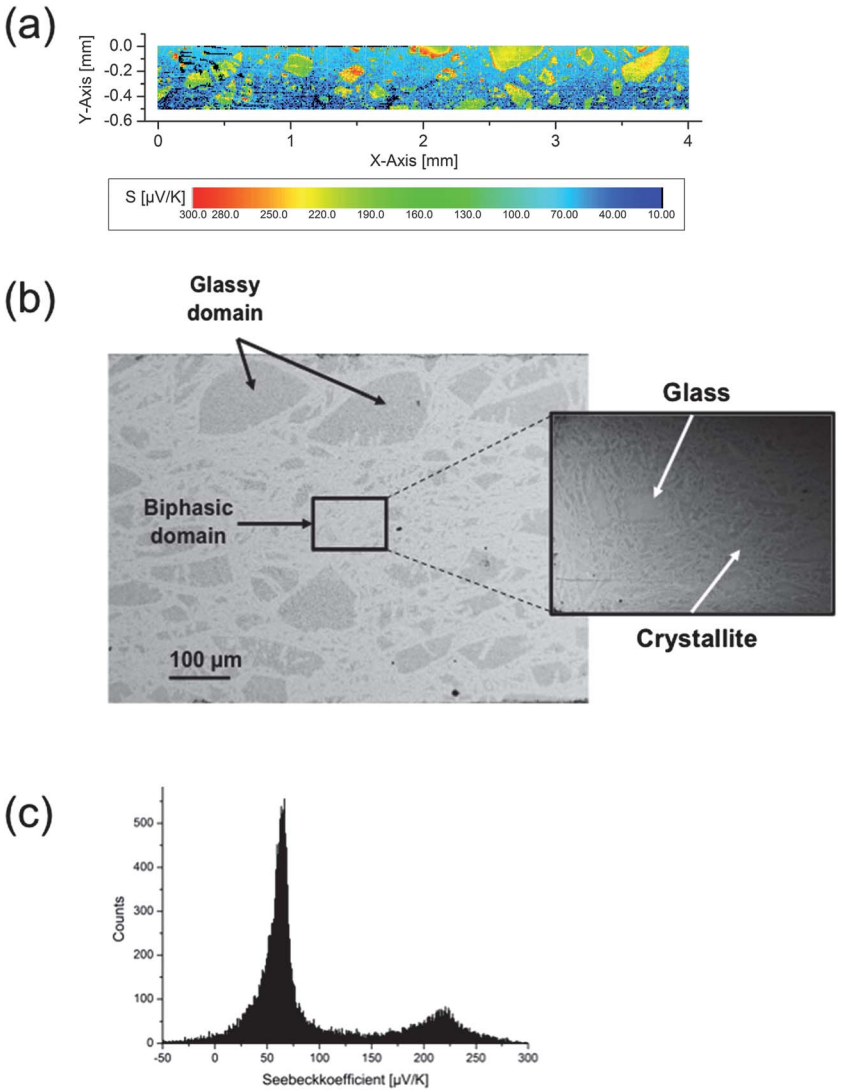

Fig. 12 (a) Mapping of the Seebeck coefficient (4 × 0.5 mm^2) of the glass–ceramics (423 K, 100 MPa, 30 min), (b) corresponding SEM photograph with chemical contrast (BSE) between the glassy phase (dark grey) and the crystalline phase (light grey), (c) distribution of thermoelectric power values on the whole cartography (a).

opposite sign of the contribution to the thermopower of both carriers. In the present case, if β-As_2Te_3 indeed behaves as an n-type semiconductor as suggested by Scheidemantel *et al.*,[20] its contribution to α would then partially cancel that of the amorphous phase, thereby decreasing the overall α values.

To further investigate this last possibility, thermopower mapping of the surface of glass–ceramic compounds was carried out. Fig. 12a shows a map realized on a 4 × 0.5 mm^2 surface area on the glass–ceramics obtained with the SPS parameters 423 K, 100 MPa and 30 min for which both amorphous and biphasic phases coexist (Fig. 12b). The distribution of the thermopower values, depicted in Fig. 12c, clearly indicates contributions from two distinct phases: one coming from a phase with high positive α values and a second with lower α values. The observed two-peak structure of the recorded signal may thus correspond to the amorphous and crystalline domains, respectively. Considering the average effect of the thermopower mapping due to the presence of dendritic domains of size below the resolution of the instrument, the tendency of the low α values towards negative values might indicate an intrinsic n-type behavior of the β-As_2Te_3 crystals.

The presence of a substantial crystalline fraction in the glassy matrix does not lead to drastic changes in specific heat C_p that amount to 0.25 J g^{-1} K^{-1} at 300 K regardless of the crystalline fraction. The thermal conductivity values, listed in Table 1, clearly increase concomitantly with the crystalline fraction: on going from the pure amorphous phase to the most crystallized sample, λ increases from 0.2 to 1.1 W m^{-1} K^{-1} at 300 K. This change towards higher values casts doubt on the validity of the assumption made in ref. 30 where a value measured in the $Ge_{20}Te_{80}$ glassy material has been used to estimate the *ZT* value of the Cu-containing samples (glass and glass–ceramics samples). The actual *ZT* value is likely to be significantly lower than the estimation given (0.2 at 300 K). Note that such a trend with the crystalline fraction is not confined to the present glass–ceramics and has been already observed in oxide glass–ceramics.[21]

These results provide an alternative way to estimate the crystalline fraction in the glass–ceramic samples. Within the effective-medium approach developed by Landauer[31] to model the thermal conductivity of composite materials, the thermal conductivity of the glass–ceramic samples composed of crystallized and amorphous phases can be expressed as

$$\lambda_{crys} = \frac{2\lambda_{exp}{}^2 - \lambda_{exp}\lambda_{glass}(3f_{glass} - 1)}{\lambda_{glass} + \lambda_{exp}(3f_{crys} - 1)} \quad (4)$$

where λ_{crys} is the thermal conductivity of the β-As_2Te_3 phase, λ_{glass} is the thermal conductivity of the pure amorphous compound, f_{glass} is the volume fraction of the amorphous phase and $f_{crys} = 1 - f_{glass}$ is the volume fraction of the crystallized phase. Assuming that the thermal conductivity of β-As_2Te_3 is $\lambda_{crys} = 4.0$ W m^{-1} K^{-1} and using the experimental values of $\lambda_{crys/glass}$ and λ_{glass}, the volume fraction of the crystallized phase f_{crys} may be inferred.[29] The values obtained by this model, and listed in Table 1, indicate a rather non-linear increase in the crystalline fraction when the dwell time increases. The maximum crystalline fraction that amounts to 43% is obtained for the longest dwell time.

The highest power factor ($P \approx 260$ μW K^{-2} m^{-1} at $T = 300$ K) was achieved in the glass–ceramics exhibiting the highest crystalline fraction. Combined with the thermal conductivity values, this leads to a *ZT* value of ~0.08 at 300 K that increases to 0.14 at 365 K. This value remains low compared to that of Bi_2Te_3-based materials considered as reference materials for room temperature applications. This limitation in the *ZT* enhancement may result from the balance between the positive influence of crystallized β-As_2Te_3 on the electrical resistivity and its detrimental effect on the thermopower. Further optimization of the thermoelectric performance might be achieved provided p-type crystals in an intrinsically p-type glassy matrix could be grown.

4 Conclusion

The microstructure and thermal stability of the $Cu_{15}As_{30}Te_{55}$ glass and its corresponding glass–ceramics analogues were investigated by means of DSC, X-ray diffraction and temperature-dependent neutron diffraction experiments. Transport properties measurements were further carried out to determine the influence of partial crystallization on the thermoelectric properties. The SPS-controlled process was demonstrated to be an efficient tool to crystallize a substantial fraction of the glassy matrix. The metastable β-As_2Te_3 phase was found to crystallize first through the glassy matrix as the dwell time or the temperature of the SPS treatment increases. While this phase undergoes a transition to the stable α-As_2Te_3 phase above 409 K *i.e.* at temperatures below that of the SPS treatment, the metastable β phase is found to be solely present in the glass–ceramics samples regardless of the SPS parameters used. The applied pressure and/or internal stresses during crystal growth likely play a role in the stabilization of this phase. The presence of crystallized domains has a strong and beneficial influence on the electrical resistivity that decreases by four orders of magnitude. This result provides a proof-of-principle showing the potential of this approach in tuning the electrical conduction in chalcogenide-based glasses. Yet, our study also suggests that the nature of the crystalline phase is essential in optimizing the thermoelectric efficiency. In the present case, the crystallization of β-As_2Te_3 lowers the thermopower values possibly due to an intrinsic n-type behavior suggested by thermopower mapping. The *ZT* values are nevertheless enhanced in the glass–ceramic samples reaching 0.14 at 365 K. The control of the type of conduction of the crystalline phase appears crucial to improve the thermoelectric efficiency of glass–ceramic compounds. This may be realized *via* changing and/or doping the initial glass composition and will be at the core of forthcoming studies.

Acknowledgements

The authors would like to acknowledge the financial support from the French National Agency (ANR) in the frame of its programme "PROGELEC" (Verre Thermo-Générateur "VTG"). G. D. also acknowledges the Limousin Region for its financial support through the FEDER program. E. B. L. and A. P. G. acknowledge the support of FCT, Portugal under the contract no. PTDC/CTM/102766/2008.

References

1 A. F. Ioffe, in *Semiconductor Thermoelements and Thermoelectric Cooling*, Infosearch, London, 1957.
2 G. J. Snyder and E. S. Toberer, *Nat. Mater.*, 2008, **7**, 105.
3 D. M. Rowe, in *Thermoelectrics Handbook: Macro to Nano*, CRC/Taylor & Francis, Boca Raton, FL, 2006.
4 K. Biswas, J. He, I. D. Blum, C.-I. Wu, T. P. Hogan, D. N. Seidman, V. P. Dravid and M. G. Kanatzidis, *Nature*, 2012, **489**, 414.
5 J. He, J. Androulakis, M. G. Kanatzidis and V. P. Dravid, *Nano Lett.*, 2012, **12**, 343.
6 Y. Pei, N. A. Heinz, A. LaLonde and G. J. Snyder, *Energy Environ. Sci.*, 2011, **4**, 3640.
7 Y. Pei, J. Lensch-Falk, E. S. Toberer, D. L. Medlin and G. J. Snyder, *Adv. Funct. Mater.*, 2011, **21**, 241.
8 O. Bubnova, Z. Ullah Khan, A. Malti, S. Braun, M. Fahlman, M. Berggren and X. Crispin, *Nat. Mater.*, 2011, **10**, 429.
9 K. C. See, J. P. Feser, C. E. Chen, A. Majumdar, J. J. Urban and R. A. Segalman, *Nano Lett.*, 2010, **10**, 4664.
10 M. He, J. Ge, Z. Lin, X. Feng, X. Wang, H. Lu, Y. Yang and F. Qiu, *Energy Environ. Sci.*, 2012, **5**, 8351.
11 D. Souri, *J. Phys. D: Appl. Phys.*, 2008, **41**, 105102.
12 L. J. Van der Pauw, *Philips Res. Rep.*, 1958, **13**, 1.
13 R. T. Littleton IV, J. Jeffries, M. Kaeser, M. Long and T. M. Tritt, *Mater. Res. Soc. Symp. Proc.*, 1999, **545**, 137.
14 D. Platzek, G. Karpinski, C. Stiewe, P. Ziolkowski, C. Drasar and E. Müller, in *Proceedings of the 24th International Conference on Thermoelectrics*, IEEE, New York, 2005, p. 13.
15 A. Hruby, *Czech. J. Phys.*, 1972, **B22**, 1187.
16 T. Ozawa, *Polymer*, 1971, **12**, 150.
17 M. N. Rahaman, in *Sintering of ceramics*, CRC/Taylor and Francis, 2008, p. 47.
18 U. Anselmi-Tamburini, S. Gennari, J. E. Garay and Z. A. Munir, *Mater. Sci. Eng., A*, 2005, **394**, 139.
19 E. Marquez, J. Vazquez, N. de la Rosa-Fox, P. Villares and R. Jimenez-Garay, *J. Mater. Sci.*, 1988, **23**, 1399.
20 T. J. Scheidemantel, J. F. Meng and J. V. Badding, *J. Phys. Chem. Solids*, 2005, **66**, 1744.
21 H. W. Shu, S. Jaulmes and J. Flahaut, *J. Solid State Chem.*, 1988, **74**, 277.
22 H. W. Shu, S. Jaulmes and J. Flahaut, *Mater. Res. Bull.*, 1986, **21**, 1509.
23 S. Toscani, J. Dugue, R. Ollitrault and R. Ceolin, *Thermochim. Acta*, 1991, **186**, 247.
24 G. K. Williamson and W. H. Hall, *Acta Metall.*, 1953, **1**, 22.
25 J. Rodriguez-Carvajal, *Physica B*, 1993, **192**, 55.
26 I. Lucks, P. Lamparter and E. J. Mittemeijer, *J. Appl. Crystallogr.*, 2004, **37**, 300.
27 A. P. Gonçalves, E. B. Lopes, G. Delaizir, J. B. Vaney, B. Lenoir, A. Piarristeguy, A. Pradel, J. Monnier, P. Ochin and C. Godart, *J. Solid State Chem.*, 2012, **193**, 26.
28 T. C. Harman, B. Paris, E. Miller and H. L. Goering, *J. Phys. Chem. Solids*, 1957, **2**, 181.
29 T. J. Scheidemantel and V. Badding, *Solid State Commun.*, 2003, **127**, 667.
30 A. P. Gonçalves, E. B. Lopes, O. Rouleau and C. Godart, *J. Mater. Chem.*, 2010, **20**, 1516.
31 R. Landauer, *J. Appl. Phys.*, 1952, **23**, 779.

